

Closed-Form Modelling of Vertical Cylinder Quality in Support of Laser Scanner Network Design

Derek D LICHTI, Canada

Key words: Engineering survey, laser scanning, photogrammetry, network design, cylinder modelling

SUMMARY

Geometric network design has long been acknowledged as an important process for precise geodetic and photogrammetric measurement projects and attention to the design of terrestrial laser scanner networks has increased in recent years. First order design (FOD) is concerned with determining network configuration that includes the instrument locations, scan overlap and target locations needed to meet project quality specifications. FOD design can be performed by simulating the environment to be measured and evaluating the suitability of candidate instrument locations. A built environment such as a complex structure or industrial facility generally comprises many key elements that can be modelled as geometric primitives such as planes (walls, floor and ceiling) and cylinders (pipes and columns). To evaluate the quality of geometric models of these objects at the design stage, the generation of simulated observations may be necessary. These data can be generated by ray casting, which can be a computationally expensive process. In order to avoid these computations, model quality can instead be evaluated in closed form. With prior knowledge of the simulated object location relative to the candidate instrument locations and the instrument specifications, the covariance matrix of model parameters can be evaluated without simulating observations. This is achieved by modelling the geometric distribution of range observations in 2D angular space with a function that is introduced into the least-squares normal equations. This paper presents the closed form modelling approach for vertical cylinders observed with a terrestrial laser scanner. Results are presented from several real laser scanner datasets. The closed-form model precision is compared with the numerical estimates obtained from the parameter covariance matrix from the least-squares estimation process. Test results indicate that the proposed method can predict parameter precision with an overall accuracy of 3%.

Closed-Form Modelling of Vertical Cylinder Quality in Support of Laser Scanner Network Design

Derek D LICHTI, Canada

1. INTRODUCTION

Laser scanning is playing an important role in 3D reality capture of the built environment thanks to the speed, density and accuracy with which datasets can be collected at complex sites. The accuracy requirement for a particular project generally dictates whether a kinematic or mobile laser scanning (MLS) system or a static, tripod-based terrestrial laser scanning (TLS) system is used. The focus of this paper is the latter, though the concepts proposed herein could conceivably be developed further to suit kinematic systems.

The importance of network design for TLS surveys is well recognized. In the geomatics/photogrammetry/geodesy communities, geometric network design is decomposed into the four design problems described by Grafarend (1974). Zero order design (ZOD) is concerned with datum definition, first order design (FOD) focuses on the geometric configuration and second order design (SOD) is devoted to the stochastic model. Third order design (TOD) refers to network densification, if necessary.

TLS network design is known by different names in other disciplines, such as viewpoint (VP) planning or planning for scanning (P4S; Aryan et al., 2021) and does not necessarily follow the same systematic decomposition into the ZOD, FOD, SOD and TOD problems. However, many of the essential elements are treated. The ZOD problem is typically addressed with pre-surveyed targets, which also solves the problem of scan orientation, or by selection of a master scan to which all other scans are registered using cloud-to-cloud methods. Instrument selection is a major factor governing SOD. Since the capital cost of TLS instruments can be high, SOD does not receive as much attention as FOD. Simply put, the stochastic model is governed largely by the availability of a single instrument.

FOD garners most of the attention in TLS network design. Given a measurement volume, the FOD task is to (automatically) determine the minimum number of instrument setup locations or viewpoints in order to minimize data collection and processing costs. Traditional design criteria include precision (confidence regions for network parameters) and reliability (network robustness). TLS network design also includes completeness and overlap. Completeness is the proportion of site that is covered by the composite point cloud. It is a function of site geometry and complexity and the instrument locations. It can be thought of as an exercise in avoiding occlusions as much as possible. Instrument capability is not a major factor since many modern scanners feature a near spherical field of view. Overlap is an indicator of the redundancy of data coverage, which is primarily required for the registration process. A value of 0.2 has been suggested (Ahn and Wohn, 2016) and adopted by others (Chen et al., 2018).

Quality measures adopted for TLS FOD may include the level of detail and the level of accuracy (e.g., Aryan et al., 2021). The level of detail in a point cloud is a matter of information content and is governed by instrument capabilities and sampling theory, though its overall quantification is complicated by the registration of multiple scans. The level of detail can be defined in terms of angular sampling interval or the linear increment it subtends, which are most useful from the perspective of a single scan, or by point density quantified by the number of observation points per unit area. The laser beamwidth can also influence information content since the projected spot acts analogously to a sampling aperture in a digital camera (Lichti and Jantsho, 2006).

Point cloud accuracy is influenced by many factors including the instrumentation (noise and calibration quality), site conditions (atmospheric, surface reflectivity, geometry, etc.) and point cloud registration quality. Aryan et al. (2021) give an example of published level of accuracy requirements for scanning projects. Point cloud accuracy can only be predicted with precision measures at the design stage. If all potential error sources are accounted for, then the precision of a radiated point can be readily computed by variance propagation. One can argue, however, that individual point precision is of less interest than the precision of the parameters of a model element, such as a plane or a cylinder, that is derived from a point cloud to construct the final site model.

Many approaches for TLS network design exist, e.g. (Ahn and Wohn, 2016; Chen et al., 2018; Dehbi et al., 2021; Heidari Mozaffar and Varshosaz, 2016; Jia and Lichti, 2019; Qiu et al., 2021; Soudarissanane and Lindenbergh, 2012). They can be broadly classified into those that assume the existence of a prior model and those that do not. The latter is a common problem in robotics where the system must build the model as it moves through its environment. In the former case, which is of primary interest here, a prior CAD model forms the foundation of the design. Though each published method has its own unique features, the following is intended to be a general description of the process. It is recognized that it is well informed by our prior experience in this interesting subject (Jia and Lichti, 2019).

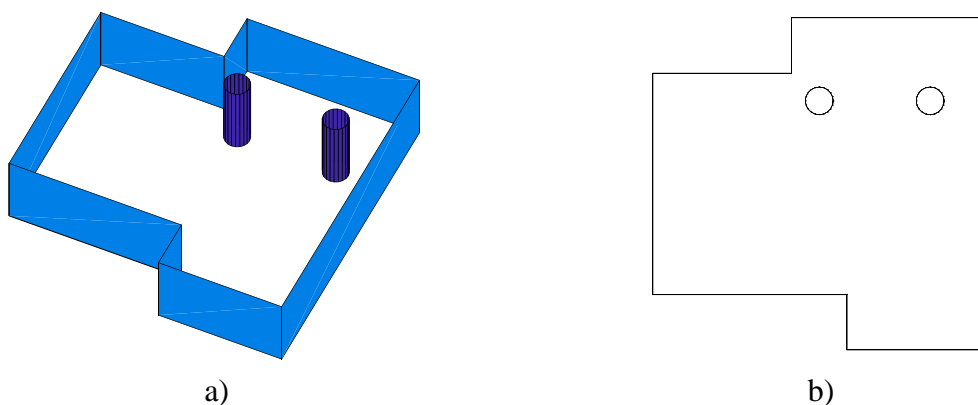


Figure 1. Artificial environment to be scanned in a) 3D and b) 2D.

Figure 1a represents an existing model of an artificial site to be scanned. Typically, the analysis is performed in 2D rather than 3D, so Figure 1b shows a plan view of the site. The walls and other important elements are decomposed into smaller entities, i.e. line segments. The workspace is the area in which the TLS instrument can be placed for data capture. It is discretized into a set of candidate viewpoint locations (Figure 2a). This sampling may be performed at several resolutions (Jia and Lichti, 2019). The data quality of each object with line-of-sight visibility from a given VP is analyzed (Figure 2b). Viewpoints are ranked in some way; greedy algorithm methods are most common according to Aryan et al. (2021). Some segments may contribute a higher weight to the ranking according to their importance. The set of VPs giving complete coverage within the design constraints defines the TLS network (Figure 2c). The design may also include the best path between the chosen viewpoints as well as target locations.

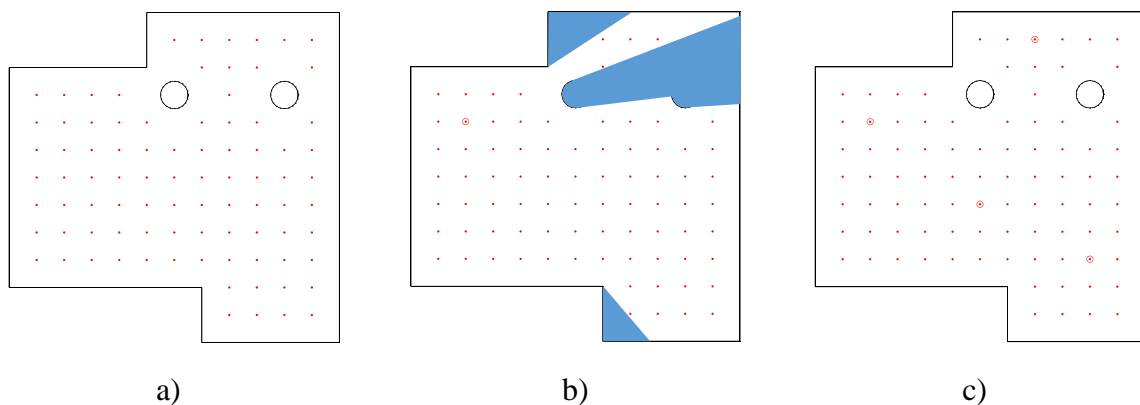


Figure 2. a) Set of all candidate viewpoints (red dots). b) Visibility constraints (occlusions shown as blue shading) from a candidate viewpoint (circled red dot). c) Final network of viewpoints (circled red dots).

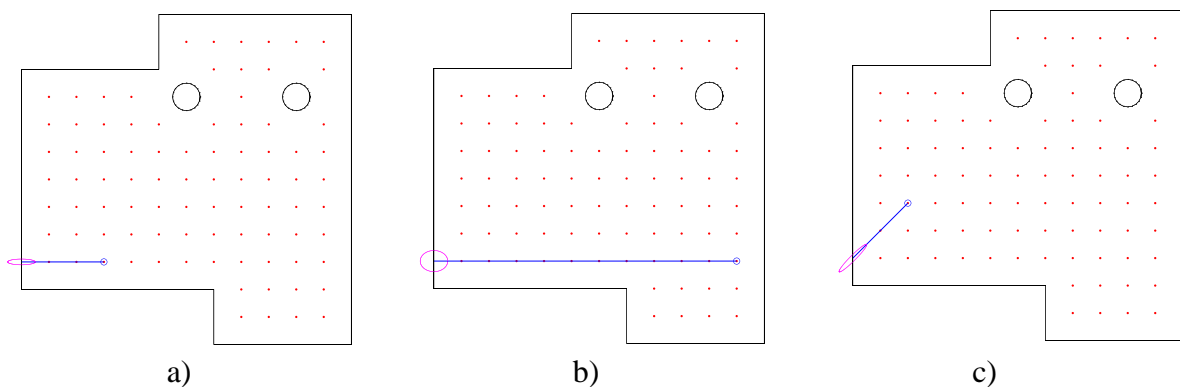


Figure 3. a), b) Range and c) incidence angle impacts on point precision. Candidate view points are indicated by blue circles. Observation rays are indicated by the blue lines and point confidence regions are indicated by the magenta ellipses.

Model precision is of course a function of observation precision. In FOD methods for TLS networks, data precision is usually simplified to be a function of a few criteria. Minimum and

maximum range constraints are necessary to accommodate recommended instrument operation conditions as well as the degradation of point precision with range (Figures 3a and 3b). Range precision also degrades at high incidence angles (Figure 3c). The combined effects of distance, incidence angle and reflectivity can be collectively accounted for a function of return signal intensity (Wujanz et al., 2017). The incidence angle effect is shown separately for illustrative purposes.

Data precision is also strongly influenced by the distribution of the observations on a scanned object. The distribution of the observations is governed by scanner-object geometry and the instrument capability. Figure 4 shows a line representing a wall segment in the example that has been scanned from two different candidate viewpoints. The histograms show the distribution of x coordinates along the line, which clearly depend on VP location. For this example, a least-squares estimate of the line segment parameters (slope, m, and intercept, b) and their covariance matrix were derived using homogeneous Cartesian y coordinate observation precision. The x-coordinates were assumed to be error free. The precision of the y-coordinates along line element is given by

$$\sigma_{\hat{y}} = \pm c \sqrt{x^2 \sigma_m^2 + \sigma_b^2} \quad (1)$$

where σ_b^2 and σ_m^2 are variances of the estimated offset and slope parameters, c is the scale factor determined by the confidence level; and $\sigma_{\hat{y}}$ is the standard deviation of the adjusted line segment. (Note that the x-coordinates were reduced to their centroid to ensure no correlation between m and b.)

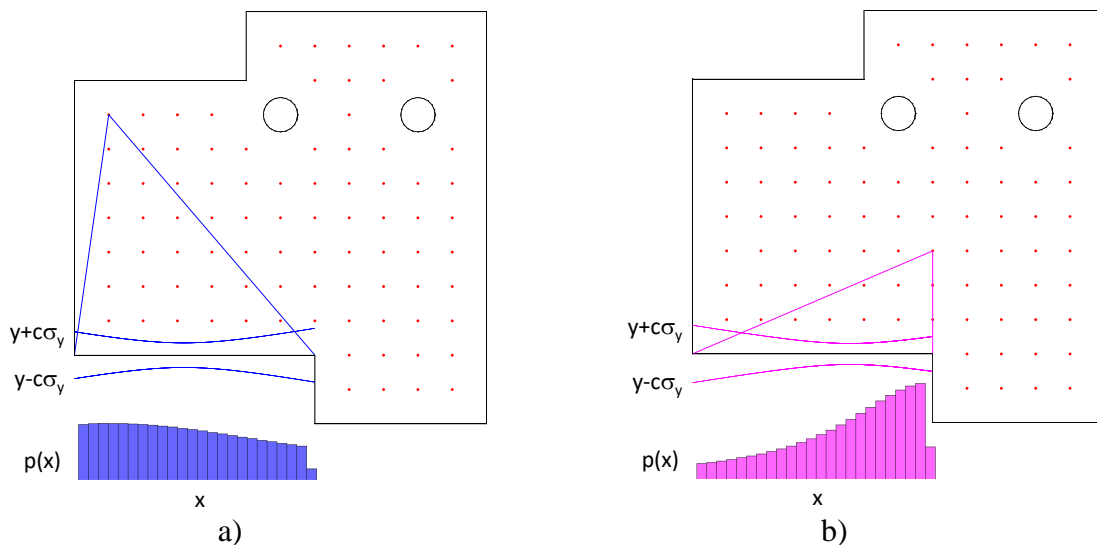


Figure 4. The impact of the coordinate observation distribution (histograms) on model precision (confidence regions). The candidate viewpoints are located at the intersection of the observation rays to the horizontal line end points.

The differences in the two confidence regions illustrate the strong impact that the distribution of the observations can have on object precision. The exact mechanism by which the distribution of the observations influences precision can be determined at least two ways: by simulation and in closed form. This paper presents a new, closed-form approach to model the observation distribution and determine parameter precision with specific focus on vertical cylinders. The theory of this method is presented in the next section. Experiments designed to validate the method with real scanner data are described in Section 3. The results are presented and discussed in Section 4, which is followed by concluding remarks and avenues for future research.

2. METHODS

Both the discrete and the closed-form methods precision estimation methods rely upon a simple model for how a TLS instrument collects spherical coordinates of a scene. A scanner can be thought of as a uniform sampling device, not unlike a digital camera. The latter features a lens that collects light and focuses it onto a solid state imaging sensor. The sensor is a rectangular grid having uniform sampling increments, Δx and Δy , between individual detector sites (Figure 5a). A TLS instrument collects range measurements in discrete angular increments, $\Delta\theta$ and $\Delta\alpha$, (Figure 5b) by two orthogonal beam deflection mechanisms.

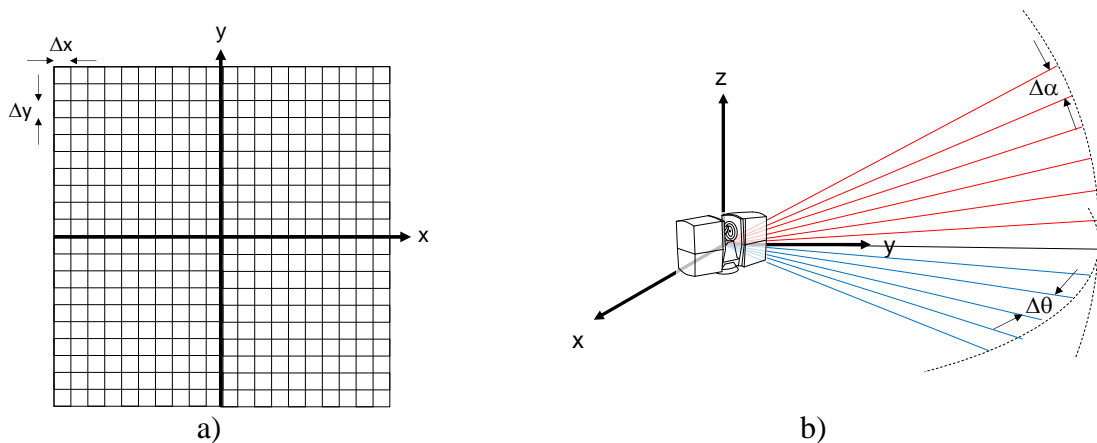


Figure 5. a) Solid state imaging and b) TLS sampling geometries.

In the discrete simulation approach, ray casting is performed from a VP to the model. Artificial rays are projected from the instrument location over the model domain according to the uniform angular sampling lattice. This produces a set of Cartesian coordinate observations on each object. These in turn are used to construct the least squares normal equations matrix that is inverted to determine the covariance matrix of object parameters, from which confidence regions can be constructed.

An alternate approach computes the covariance matrix of parameters in closed form. The development of this method begins with the functional model of the object and the least-squares

solution for its parameters given a set of discrete point observations. A nominally vertical cylinder parameterized in the instrument coordinate system is used as an example:

$$f = u^2 + v^2 - r^2 = 0 \quad (2)$$

where r is the cylinder radius. The rotated and translated coordinates (u, v) are related to the Cartesian coordinates from the scanner (x, y, z) by linear transformation

$$\begin{pmatrix} u \\ v \\ w \end{pmatrix} = \mathbf{R}_2(\phi) \mathbf{R}_1(\omega) \begin{pmatrix} x - x_c \\ y - y_c \\ z \end{pmatrix} \quad (3)$$

where (x_c, y_c) are the coordinates of the cylinder; (ω, ϕ) are the two tilt angles of the cylinder's vertical axis; and (ρ, θ, α) are the spherical coordinates collected by the scanner that are related to the Cartesian coordinates as follows:

$$\begin{pmatrix} x \\ y \\ z \end{pmatrix} = \begin{pmatrix} \rho \sin \theta \cos \alpha \\ \rho \cos \theta \cos \alpha \\ \rho \sin \alpha \end{pmatrix} \quad (4)$$

The general linearized form of Equation 2 is given by (Vaníček and Krakiwsky, 1982)

$$\mathbf{A}\hat{\boldsymbol{\delta}} + \mathbf{B}\hat{\mathbf{v}} + \mathbf{w} = \mathbf{0} \quad (5)$$

where \mathbf{A} and \mathbf{B} are the design matrices of partial derivatives of f taken with respect to the parameters and the spherical observations, respectively; \mathbf{w} is the misclosure vector; $\hat{\boldsymbol{\delta}}$ is the vector of corrections to the approximate cylinder parameter values; and $\hat{\mathbf{v}}$ is the vector of residuals for the spherical observations.

The least-squares normal equations are given by

$$\begin{aligned} \mathbf{A}^T \mathbf{M}^{-1} \mathbf{A} \hat{\boldsymbol{\delta}} &= -\mathbf{A}^T \mathbf{M}^{-1} \mathbf{w} \\ \mathbf{N} \hat{\boldsymbol{\delta}} &= -\mathbf{u} \end{aligned} \quad (6)$$

where

$$\mathbf{M} = \mathbf{B} \mathbf{P}^{-1} \mathbf{B}^T \quad (7)$$

Assuming there is no correlation between observations and the variance factor is unity, the weight matrix, \mathbf{P} , is diagonal and is given by the inverse of the covariance matrix of observations, \mathbf{C}

$$\mathbf{P} = \mathbf{C}^{-1} = \text{diag} \left(\frac{1}{\sigma_{\rho_1}^2} \quad \frac{1}{\sigma_{\theta_1}^2} \quad \frac{1}{\sigma_{\alpha_1}^2} \quad \frac{1}{\sigma_{\rho_2}^2} \quad \frac{1}{\sigma_{\theta_2}^2} \quad \frac{1}{\sigma_{\alpha_2}^2} \quad \dots \right) \quad (8)$$

The covariance matrix of parameters, \mathbf{C}_x , is obtained in the usual way by inverting the normal equations matrix, \mathbf{N}

$$\mathbf{C}_{\hat{\mathbf{x}}} = \mathbf{N}^{-1} = (\mathbf{A}^T \mathbf{M}^{-1} \mathbf{A})^{-1} \quad (9)$$

$$= \begin{pmatrix} \sigma_{x_c}^2 & \sigma_{x_c y_c} & \sigma_{x_c \omega} & \sigma_{x_c \phi} & \sigma_{x_c r} \\ & \sigma_{y_c}^2 & \sigma_{y_c \omega} & \sigma_{y_c \phi} & \sigma_{y_c r} \\ & & \sigma_{\omega}^2 & \sigma_{\omega \phi} & \sigma_{\omega r} \\ & & & \sigma_{\phi}^2 & \sigma_{\phi r} \\ \text{sym} & & & & \sigma_r^2 \end{pmatrix}$$

The method thus far represents the least-squares solution for the cylinder parameters from discrete data. To develop the closed-form approach, the weight matrix is redefined to include the function $p(\theta, \alpha)$ that describes the distribution of the angular observations.

$$\mathbf{P} = \text{diag} \left(\frac{p(\theta_1, \alpha_1)}{\sigma_{\rho_1}^2} \quad \frac{p(\theta_1, \alpha_1)}{\sigma_{\theta_1}^2} \quad \frac{p(\theta_1, \alpha_1)}{\sigma_{\alpha_1}^2} \quad \dots \right) \quad (10)$$

This function should satisfy two conditions

$$p(\theta, \alpha) > 0 \quad (11)$$

and

$$\int_{-\infty}^{\infty} \int_{-\infty}^{\infty} p(\theta, \alpha) d\theta d\alpha = 1 \quad (12)$$

The normal equations (Equation 6) are constructed with the newly defined \mathbf{P} (Equation 10) and are multiplied by $\Delta\theta\Delta\alpha$

$$\Delta\theta\Delta\alpha \mathbf{N} \hat{\boldsymbol{\delta}} = -\Delta\theta\Delta\alpha \mathbf{u} \quad (13)$$

where

$$\Delta\theta = \frac{\theta_2 - \theta_1}{m} \quad (14)$$

$$\Delta\alpha = \frac{\alpha_2 - \alpha_1}{n} \quad (15)$$

and m is the number of vertical profiles (i.e. the number of horizontal direction increments); and n is the number of observations per profile (elevation angle increments).

Finally, the limit as $m, n \rightarrow \infty$ is taken. To examine the result of these developments, element (1,1) of \mathbf{N} will be inspected more closely. The analytical form of element \mathbf{N}_{11} follows from multiplication of the individual terms of \mathbf{A} , \mathbf{B} and \mathbf{P} . Under the limit operation, the summations become integrals:

$$\begin{aligned} \lim_{m, n \rightarrow \infty} \Delta\theta\Delta\alpha\mathbf{N}_{11} &= \lim_{m, n \rightarrow \infty} \Delta\theta\Delta\alpha \sum_i^m \sum_j^n \frac{p(\theta_i, \alpha_j) u_{ij}^2 \cos^2 \phi}{\left(\frac{\partial f}{\partial \rho}\right)^2 \sigma_{\rho_{ij}}^2 + \left(\frac{\partial f}{\partial \theta}\right)^2 \sigma_{\theta_i}^2 + \left(\frac{\partial f}{\partial \alpha}\right)^2 \sigma_{\alpha_j}^2} \\ &= \lim_{m, n \rightarrow \infty} \Delta\theta\Delta\alpha \sum_i^m \sum_j^n \frac{p(\theta_i, \alpha_j) u_{ij}^2 \cos^2 \phi}{L_{ij}} \\ &= \int_{\theta_1}^{\theta_2} \int_{\alpha_1}^{\alpha_2} \frac{p(\theta, \alpha) u^2 \cos^2 \phi}{L} d\theta d\alpha \end{aligned} \quad (16)$$

where

$$L_{ij} = \left(\frac{\partial f}{\partial \rho}\right)^2 \sigma_{\rho_{ij}}^2 + \left(\frac{\partial f}{\partial \theta}\right)^2 \sigma_{\theta_i}^2 + \left(\frac{\partial f}{\partial \alpha}\right)^2 \sigma_{\alpha_j}^2 \quad (17)$$

The observation distribution function is modelled to be uniform on the angular intervals indicated by Equations 14 and 15. This is reasonable assumption given that the scanner sampling is uniform and occurs in two orthogonal directions. Thus, Equation 16 simplifies to

$$\frac{1}{(\theta_2 - \theta_1)(\alpha_2 - \alpha_1)} \int_{\theta_1}^{\theta_2} \int_{\alpha_1}^{\alpha_2} \frac{u^2 \cos^2 \phi}{L} d\theta d\alpha \quad (18)$$

Prior to integration, the expression for range to points on the surface cylinder as a function of the angles (θ, α) is substituted into Equation 18. It is obtained by substitution of Equation 4 into

Equation 2 and solving for ρ . This procedure is also applied to the other elements of the normal equations matrix.

This demonstrates how the elements of the normal equations matrix can be evaluated with an integral instead of a summation. Therefore, the ray casting operation to generate a set of simulated observations is not necessary. If the functional model is simple, such as a 2D regression line parameterized in terms of Cartesian coordinates, then the integrals can be easily evaluated (Lichti et al., 2021). If the expressions are more complex, as is the case here, then numerical integration is required. Once all integrals have been evaluated, the parameter covariance matrix can be obtained by inversion as per Equation 9.

3. EXPERIMENTS

A set of experiments was performed to examine the accuracy of vertical cylinder parameter precision estimated by the closed-form equations method. Real data of several different cylinders were collected by TLS. The covariance matrix of parameters was evaluated by two methods: the “conventional” method using the discrete observations; and by the integral method. Accuracy was quantified by the per cent difference of the standard deviations estimated with the proposed method. The standard deviations derived from the discrete observation data served as the reference for the comparison.

TLS data of seven cylinders (Figure 6) having different radii and made from different materials (steel, concrete, PVC) having different finishes (painted and unpainted) were used for the experiments. Cylinders 1 to 6 are indoors and were scanned in controlled environments (21 °C). Cylinder 7, a disused industrial tower, is outdoors. It was scanned in overcast conditions at 14 °C. Many scans of these and other cylinders were captured at different standoff distances and angular resolutions. Results from nine scans are presented herein. Cylinder 1 was scanned with a Leica BLK360 whereas the others were captured with a Leica HDS6100. The cylinder point clouds were cropped such that the upper and lower data boundaries had constant elevation angle (α). All datasets were highly redundant, with the number of points ranging from 29447 to 209350, and had good coverage along the cylinder length. The overall range of the z coordinates ranged from 1.17 m to 3.58 m. Other relevant information about the scans including the nominal standoff distance ($dist$) and the radius is given in Table 1.

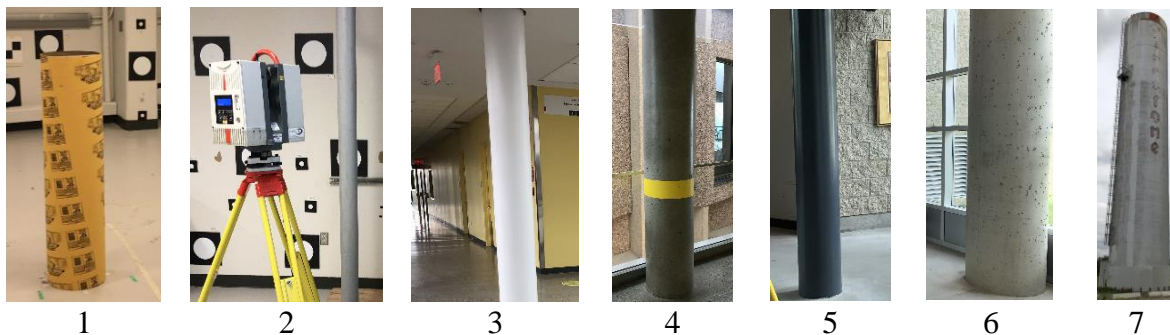


Figure 6. Scanned cylinders.

Table 1. The cylinder used, the nominal radius and the nominal standoff distance for each scan.

Scan	1	2	3	4	5	6	7	8	9
Cylinder	1	2	3	4	5	6	6	7	7
r (m)	0.15	0.06	0.17	0.23	0.16	0.38	0.38	3.67	3.67
dist (m)	3.0	3.0	5.0	3.0	3.0	1.4	4.5	1.0	2.0

The approximate cylinder parameter values for each scan were determined by manual analysis of the point clouds. The covariance matrix of cylinder parameters was determined by two methods: the discrete form using all observation points captured from a single scan location, and the continuous form. The discrete-form covariance matrix was multiplied by the number of point observations to allow direct comparison with the covariance matrix determined from the continuous equation.

4. RESULTS

The continuous model standard deviations are presented for each of the nine scans in Table 2. For most scans, the position and radius precision is sub-centimetre. The exception are scans 8 and 9, which were of the large-radius (3.67 m) cylinder 7. At such close ranges (1 m and 2 m), only a small proportion of the circumference can be scanned, so the solution is inherently weaker. Tilt angle precision ranges between 0.1° and 0.3° .

Table 2. Cylinder parameter standard deviations, continuous model estimation.

Scan	1	2	3	4	5	6	7	8	9
σ_{x_c} (mm)	5	2	3	2	3	2	4	23	19
σ_{y_c} (mm)	4	5	7	5	5	4	7	9	5
σ_ω ($^\circ$)	0.32	0.19	0.18	0.12	0.22	0.13	0.11	0.27	0.26
σ_ϕ ($^\circ$)	0.25	0.28	0.32	0.18	0.30	0.17	0.15	0.13	0.10
σ_r (mm)	4	4	6	4	4	4	6	24	18

The accuracy of the continuous precision estimates was assessed by comparing the results in Table 2 with the discrete estimates (not shown). As mentioned, the latter were considered as the ground truth. The differences expressed as the percentage of the discrete standard deviation are given in Table 3 and range from -16% to 3%. The mean values for each parameter range from -6% to -1% and the overall average computed from all 45 estimates is quite small at -3%. This close agreement suggests that the accuracy of the continuous method is very high. The negative sign of the differences indicates that the continuous model precision is slightly optimistic. The largest difference in terms of magnitude is -16%. This and the other large-magnitude differences are between one of the position coordinates and the radius. Exactly which parameter varied between x_c and y_c depending on the scan geometry. This is believed to be due to the inherent high correlation that exists between these parameters. The smaller differences may be due to deviations of the actual distribution of the angular observations from the uniform model.

Table 3. Per cent difference in cylinder parameter standard deviations and overall mean.

Scan	1	2	3	4	5	6	7	8	9		Mean
σ_{xc}	-11	-5	0	0	-4	0	0	-6	-6		-3
σ_{yc}	3	-11	-1	-5	-10	-2	-2	-12	-2		-5
σ_{ω}	0	3	-3	0	0	0	0	-6	-2		-1
σ_{ϕ}	-4	-2	0	0	0	0	0	-4	0		-1
σ_r	-16	-7	0	-4	-7	-3	-2	-7	-5		-6

CONCLUSIONS AND FUTURE WORK

As built models of the built environment are often constructed from TLS scanner data. Careful planning of the scan locations is important to maximize the precision of the reconstructed objects. Rigorous planning may require simulation of dense datasets by ray casting in order to accurately estimate modeled object precision. The specific focus of this work has been vertical cylinders, which are frequently found in the built environment. This paper has presented a method to predict the precision of a modelled vertical cylinder without the need to generate a synthetic point cloud. The basis for the method is a model for the angular distribution of the range observations and the continuous form of the least-squares normal equation matrix. Testing demonstrated that the proposed method can predict parameter precision with an overall accuracy of 3%. Precision estimates from the continuous equations were slightly optimistic, which is likely due to the non-idealized distribution of the real data against which the model predictions were evaluated.

Future work will focus on a more realistic scanning limits. Vertical cylinders are typically extracted by defining lower and upper z-coordinate boundaries rather than by cropping the point cloud between constant elevation angle boundaries. The work will also be extended to other important 3D objects such as planes and spheres. Finally, objects that are not nominally vertical or are not oriented in cardinal directions must be treated to allow broader application.

ACKNOWLEDGEMENTS

Funding to support this research was provided by the Natural Sciences and Engineering Research Council (NSERC) of Canada (RGPIN-2018-03775) and the Canada Foundation for Innovation. Kate Pexman is gratefully acknowledged for assistance with the data collection.

REFERENCES

- Ahn, J., Wohn, K., 2016. Interactive scan planning for heritage recording. *Multimed Tools Appl* 75, 3655–3675. <https://doi.org/10.1007/s11042-015-2473-0>
- Aryan, A., Bosché, F., Tang, P., 2021. Planning for terrestrial laser scanning in construction: A review. *Automation in Construction* 125, 103551. <https://doi.org/10.1016/j.autcon.2021.103551>
- Chen, M., Koc, E., Shi, Z., Soibelman, L., 2018. Proactive 2D model-based scan planning for existing buildings. *Automation in Construction* 93, 165–177. <https://doi.org/10.1016/j.autcon.2018.05.010>

- Dehbi, Y., Leonhardt, J., Oehrlein, J., Haunert, J.-H., 2021. Optimal scan planning with enforced network connectivity for the acquisition of three-dimensional indoor models. *ISPRS Journal of Photogrammetry and Remote Sensing* 180, 103–116. <https://doi.org/10.1016/j.isprsjprs.2021.07.013>
- Grafarend, E.W., 1974. Optimization of Geodetic Networks. *Bolletino di Geodesia a Science Affini* 33, 351–406.
- Heidari Mozaffar, M., Varshosaz, M., 2016. Optimal Placement of a Terrestrial Laser Scanner with an Emphasis on Reducing Occlusions. *Photogram Rec* 31, 374–393. <https://doi.org/10.1111/phor.12162>
- Jia, F., Lichti, D.D., 2019. A Model-Based Design System for Terrestrial Laser Scanning Networks in Complex Sites. *Remote Sensing* 11, 1749. <https://doi.org/10.3390/rs11151749>
- Lichti, D.D., Chan, T.O., Belton, D., 2021. Linear regression with an observation distribution model. *J Geod* 95, 23. <https://doi.org/10.1007/s00190-021-01484-x>
- Lichti, D.D., Jamtsho, S., 2006. Angular resolution of terrestrial laser scanners. *Photogrammetric Record* 21, 141–160. <https://doi.org/10.1111/j.1477-9730.2006.00367>
- Qiu, Q., Wang, M., Tang, X., Wang, Q., 2021. Scan planning for existing buildings without BIM based on user-defined data quality requirements and genetic algorithm. *Automation in Construction* 130, 103841. <https://doi.org/10.1016/j.autcon.2021.103841>
- Soudarissanane, S., Lindenbergh, R., 2012. OPTIMIZING TERRESTRIAL LASER SCANNING MEASUREMENT SET-UP. *Int. Arch. Photogramm. Remote Sens. Spatial Inf. Sci.* XXXVIII-5/W12, 127–132. <https://doi.org/10.5194/isprarchives-XXXVIII-5-W12-127-2011>
- Vaníček, P., Krakiwsky, E., 1982. *Geodesy: The Concepts*. North Holland, Amsterdam.
- Wujanz, D., Burger, M., Mettenleiter, M., Neitzel, F., 2017. An intensity-based stochastic model for terrestrial laser scanners. *ISPRS Journal of Photogrammetry and Remote Sensing* 125, 146–155. <https://doi.org/10.1016/j.isprsjprs.2016.12.006>

BIOGRAPHICAL NOTES

Derek Lichti is Professor with the Department of Geomatics Engineering at the University of Calgary, Canada.

CONTACTS

Professor Derek D Lichti
Department of Geomatics Engineering
University of Calgary
2500 University Drive NW
Calgary, Alberta T2N 1N4
CANADA
Ph: +1 403 210 9495
ddlichti@ucalgary.ca